Journal of Neural Engineering

Extending the understanding of Shannon's safe stimulation limit for platinum electrodes: biphasic charge-balanced pulse trains in unbuffered saline at pH = 1 to pH = 12

To cite this article before publication: Thomas Niederhoffer *et al* 2024 *J. Neural Eng.* in press https://doi.org/10.1088/1741-2552/ad3b6a

Extending the understanding of Shannon's safe stimulation limit for platinum electrodes: biphasic charge-balanced pulse trains in unbuffered saline at pH = 1 to pH = 12

Thomas Niederhoffer [1], Anne Vanhoestenberghe [2], and Henry T. Lancashire [1,†]

[1] Department of Medical Physics and Biomedical Engineering, University College London, WC1E 6BT, UK

[2] School of Biomedical Engineering and Imaging Sciences, King's College London, UK; a.vanhoest@kcl.ac.uk

E-mail: [†] h.lancashire@ucl.ac.uk

October 2023

Abstract. *Objective:* In neural electrical stimulation, safe stimulation guidelines are essential to deliver efficient treatment by avoiding neural damage and electrode degradation. The widely used Shannon's limit, k, gives conditions on the stimulation parameters to avoid neural damage, however, underlying damage mechanisms are not fully understood. Moreover, the translation from bench testing to *in vivo* experiments still presents some challenges, including the increased polarisation observed, which may influence charge-injection mechanisms. In this work, we studied the influence on damage mechanisms of two electrolyte parameters that are different *in vivo* compared to usual bench tests: solution pH and electrolyte gelation.

Approach: The potential of a platinum macroelectrode was monitored in a three-electrode setup during current-controlled biphasic charge-balanced cathodic-first pulse trains. Maximum anodic and cathodic potential excursions during pulse trains were projected on cyclic voltammograms to infer possible electrochemical reactions.

Main results: In unbuffered saline of pH ranging from 1 to 12, the maximum anodic potential was systematically located in the oxide formation region, while the cathodic potential was located the molecular oxygen and oxide reduction

region when k approached Shannon's damage limit, independent of solution pH. The results support the hypothesis that Shannon's limit corresponds to the beginning of platinum dissolution following repeated cycles of platinum oxidation and reduction, for which the cathodic excursion is a key tipping point. Despite similar potential excursions between solution and gel electrolytes, we found a joint influence of pH and gelation on the cathodic potential alone, while we observed no effect on the anodic potential. We hypothesise that gelation creates a positive feedback loop exacerbating the effects of pH ; however, the extent of that influence needs to be examined further.

Significance: This work supports the hypothesis of charge injection mechanisms associated with stimulation-induced damage at platinum electrodes. The validity of a major hypothesis explaining stimulation-induced damage was tested and supported on a range of electrolytes representing potential electrode environments, calling for further characterisation of platinum dissolution during electrical stimulation in various testing conditions.

Submitted to: *J. Neural Eng.*

1. Introduction

Neural stimulation electrodes are used to treat a range of neuropathologies, including neurodegenerative diseases such as Alzheimer's, and to restore impaired functions, including following spinal cord injuries and hearing loss. Neural stimulation with implanted electrodes is an invasive treatment, which may be harmful, therefore safe stimulation guidelines have been established. Water electrolysis reactions are known to cause neural damage through large current flow and large pH shifts (Cogan et al.; 2016), therefore, the electrode potential should be kept within the water window (typically [-0.6 V to +0.8 V vs Ag|AgCl]). Because monophasic stimuli reached safe limits relatively rapidly due to electrode polarisation (Mortimer and Bhadra; 2018), charge-balanced biphasic stimuli were introduced to maintain the electrode potential within safe bounds (Lilly et al.; 1955; Donaldson and Donaldson; 1986b). However, a series of *in vivo* experiments in cat brains demonstrated signs of neural damage despite respecting the water window potential limits (Yuen et al.; 1981; Agnew et al.; 1983, 1986, 1989; McCreery et al.; 1988, 1990). A new safe stimulation limit was proposed by Shannon (1992) who found a relationship between stimulation parameters and observed damage described by a parameter, "k" (Shannon's parameter), according to equation 1.

$$log\ D = k - log\ Q, \tag{1}$$
$$k = log\ D + log\ Q,$$

Hence, with D = Q/S and Q = $i_c\Delta$t:

$$i_c = \frac{\sqrt{S\,10^k}}{\Delta t}. \tag{2}$$

In equations 1 and 2, D is the charge density per phase, Q is the charge per phase, i_c is the cathodic current, S is the electrode surface area, and Δt is the pulse width. Note that this expression of i_c is only valid for square cathodic pulses ($Q = i_c\,\Delta t$ is only valid if i_c is constant) and that S is the geometric surface area. k represents a diagonal line with negative slope on a plot of log(D) against log(Q),

which shifts parallel with changes in k, see Fig. 1. At $k = 1.75$ for platinum, this line divides the plot between non-damaging stimulation and damaging stimulation (Fig. 1).

The advantage of Shannon's equation 1 is the direct relationship between stimulation parameters and neural damage, reported as shrunken neurons in the vicinity of the electrode immediately after the stimulation period (McCreery et al.; 1990). In an anterior study, McCreery et al. (1988) showed that neurons which shrunk following stimulation mostly recovered one week after the end of stimulation; however, McCreery et al. argued that prolonged stimulation may have resulted in more irreversible damage to neurons. Shannon's equation does not include a number of stimulation parameters (frequency, duty cycle) and information about the electrode (geometry, roughness), which restrict the scope of application (Cogan et al.; 2016). Frequency has been showed to influence damage thresholds on retinal cells (Butterwick et al.; 2007) and in peripheral nerves (McCreery et al.; 1995). Butterwick et al. (2007) also showed that macroelectrodes and microelectrodes had different damage threshold scaling, which pushed forward a new damage limit for microelectrodes (4 nC/ph) (McCreery et al.; 2010), while Kumsa et al. (2017) showed that electrodes with areas ranging from 0.2 mm^2 to 12.7 mm^2 followed the same scaling with k. Duty cycle was also addressed, showing no damage when the charge density remained low enough even close to 100% (Kuncel and Grill; 2004), but a decrease in neuron excitability is observed at higher charge densities (Tykocinski et al.; 1995).

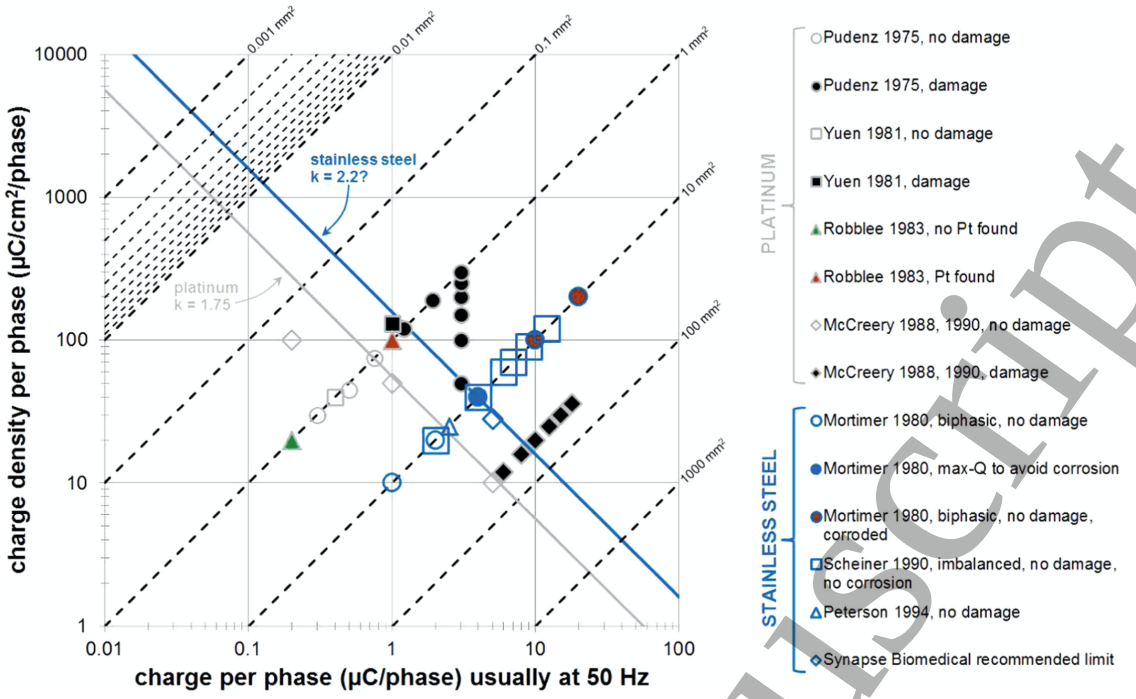

Figure 1: *Shannon's plot showing the limit between damaging (filled markers) and non damaging stimulation (empty markers) for platinum (grey line) and stainless steel (blue line). Figure reproduced from Kumsa et al. (2016), CC BY 3.0.*

Moreover, the mechanisms underlying the $k = 1.75$ damage limit were not explained by this relationship. Two theories are presented to explain neural damage following neural stimulation: neuron overstimulation leading to a loss of excitability of neurons (stimulation-induced depression of neuronal excitability or SIDNE); and production of harmful species through electrode degradation or other reactions at the electrode surface. Rather than being opposed, both theories may occur simultaneously, and the observation of one of these mechanisms does not exclude the other (Cogan et al.; 2016). These theories actually relate to different ways of measuring damage: SIDNE corresponds to a functional evaluation of damage, where one measures the activity of neurons, while the electrochemical theory corresponds to a histological evaluation of damage, where tissues are visually inspected to find traces of damage, and both are usually mutually exclusive because they cannot be performed simultaneously (Cogan et al.; 2016). Shannon's limit is based on a histological evaluation of damage, therefore, it addresses rather an electrochemical cause of neural damage and did not consider parameters such as frequency or duty

cycle, related to SIDNE. The present study addresses electrochemical mechanisms behind Shannon's limit, therefore, we will focus on electrochemical reactions at the electrode-electrolyte interface that may produce harmful species for neurons.

Platinum electrode corrosion, which releases platinum in the body was suspected to cause the damage observed by McCreery et al. (1990) as traces of platinum were found at $k \geq 1.75$ *in vitro* (McHardy et al.; 1980; Donaldson and Donaldson; 1986a) and *in vivo* (Robblee et al.; 1983), and the injection of platinum salts in brain tissue caused damage similar to that observed during stimulation (Agnew et al.; 1977). Merrill et al. (2005) proposed a mechanism to explain the emergence of platinum dissolution: as there is no control over electrode potential in current-controlled pulses, the electrode potential changes depending on the molecular arrangements at its surface. In charge-balanced biphasic stimulation, although the injected electrical charge is equal in both phases, an imbalance in charge injection mechanisms occurs due to irreversible electrochemical reactions (Musa et al.; 2011; Kumsa et al.; 2016). The imbalance between phases in irreversible mechanisms leads the electrode potential to change, positively for an cathodic imbalance (more irreversible charge during cathodic phase) and negatively for a anodic imbalance, in a process called potential ratcheting or potential slide back (Craggs et al.; 1986; Donaldson and Donaldson; 1986a; Merrill et al.; 2005; Harris et al.; 2019). Thus, $k = 1.75$ may correspond to potential ratcheting leading the electrode potential into regions favourable for platinum dissolution. Potential ratcheting can be minimised by discharging the electrodes between pulses or by using charge-imbalanced pulses (Kumsa et al.; 2019), which adapt the charge injection to avoid changing the electrode potential through excessive charge injection in the reversal phase.

Kumsa et al. (2016) developed a framework to identify the relationship between k and electrochemical reactions by monitoring the electrode potential during biphasic pulse trains and projecting the observed potentials on cyclic voltammograms, which indicate available reactions. Kumsa et al. (2016) found that exceeding the Shannon's stimulation limit $k = 1.75$ corresponded to the onset of platinum oxidation. Sulfuric

acid was used as electrolyte ; however, there are a few electrolyte parameters that may influence the charge injection mechanisms, and a fortiori damage, including pH, ions, and biological molecules (Harris et al.; 2018b,a, 2019). pH for instance is known to vary upon implantation of a microelectrode, with shifts between +0.1 and -0.6 pH units, which tend to stabilise around -0.2 (pH = 7.2) after a few minutes (Gupta et al.; 2004; Johnson et al.; 2007), and furthermore, electrical stimulation may cause local pH changes (Ballestrasse et al.; 1985; Huang et al.; 2001; Weltin and Kieninger; 2021), which may affect reaction pathways and damage. *In vivo* electrode behaviour is still poorly understood, leading to suboptimal use of electrodes' charge injection capacity (DiLorenzo et al.; 2014; Harris et al.; 2022), for example, the causes of larger electrode polarisation *in vivo* (Cogan; 2008; Renz et al.; 2018) have not been clearly identified, with safe charge injection limits between 8.7 (Leung et al.; 2014) and 24 (Vatsyayan et al.; 2021) times lower *in vivo* than *in vitro*, suggesting that other parameters may affect electrode behaviour and damage mechanisms.

The present work aims to broaden the understanding of the mechanisms behind the observed Shannon (1992) $k = 1.75$ limit by studying the influence of two electrolyte parameters: pH and gelation. pH is usually very stable in the body around 7.4 due to vairous buffer systems, however, local pH is known to vary, including during neural stimulation with shifts of -1 pH unit measured 0.2 mm away from electrodes, which may be larger close to the electrode surface (Huang et al.; 2001; Ballestrasse et al.; 1985). Unbuffered saline was chosen to study the influence of a pH shift at the electrode surface, which would have been impeded by using a buffer (Huang et al.; 2001). Since the magnitude of the pH shift at the electrode surface is not fully known, the whole pH range was covered. *In vivo* implantation introduces tortuous diffusion paths for charge carriers (Cogan; 2008), which may change reaction pathways due to reactant unavailability. We used a gelating agent (agar), which is often used in cell cultures to mimick the extracellular matrix to represent tissue structures more accurately than fluid test solutions. Such a gel electrolyte aims to model the tissue structure around electrodes in acute experiments, such as the experiments on which Shannon's limit is based

(Agnew et al.; 1983, 1986, 1989; McCreery et al.; 1988, 1990). A suitable tissue model for chronic studies would require a much denser fibrous structure to factor in fibrous encapsulation, which occurs within the first few weeks of implantation (Campbell and Wu; 2018). The secondary aim of this study is to identify which parameters in body fluids and tissues affect charge injection mechanisms. Therefore, if these parameters are shown to influence damage mechanisms, they will need to be incorporated in characteristic electrolytes when developing and testing new electrodes. The framework used to conduct this study is inspired by Kumsa et al. (2016) to precisely discriminate influential reactions based on k, the neural damage indicator.

2. Methods

2.1. Electrolytes

Unbuffered saline solutions were prepared by mixing a sodium chloride (NaCl) saline solution with hydrochloric acid (HCl) or sodium hydroxide (NaOH) to adjust pH to the desired value. Medical grade NaCl (MW: 58.45 $g.mol^{-1}$, Promega) was diluted in deionized water (DW, 15.6 $M\Omega$, Millipure system) at a concentration of 18 $g.L^{-1}$ or twice the isotonic concentration (0.9%w/v, equivalent to 9 $g.L^{-1}$). HCl (1 M, Sigma-Aldrich) and NaOH (crystals, BDH) were diluted at twice the desired concentration in DW and mixed in a 1:1 ratio with 18 $g.L^{-1}$ NaCl to have an isotonic 9 $g.L^{-1}$ solution of desired pH. Solutions were not degassed before experiments and were carried out in equilibrium with the ambient oxygen concentration (21%). Solution pH was measured before and immediately after every set of measurements (5 or 7 k-values) to detect possible chemical changes in the unbuffered electrolyte.

Agar powder was added (0.5% w/v) to the base electrolytes, and gelation was achieved by heating to boiling point followed by cooling to room temperature. pH was measured following gelation. Agar gel electrolytes were prepared with four base solution electrolytes: phosphate-buffered saline (PBS), sulfuric acid (H_2SO_4), pH 1 saline (HCl in isotonic 9 $g.L^{-1}$ NaCl) and pH 11 saline (NaOH in isotonic 9 $g.L^{-1}$

NaCl).

2.2. Pulsing experiment

Trains of 1000 biphasic current-controlled cathodic-first asymmetric charge-balanced pulses with capacitive discharge anodic balancing phase, see Fig. 3, were applied with a custom stimulator inspired from Hudak (2011) and Kumsa et al. (2016). The capacitive discharge anodic phase effectively ensures charge balancing with a capacitor connected in series with the electrodes charged in the cathodic phase and discharged in the anodic phase(Merrill et al.; 2005; Kumsa et al.; 2016). The amount of injected charge was controlled by changing the cathodic current through a transistor, acting as voltage-controlled current source (Hudak; 2011) ; cathodic currents and charge densities are given in Table 1. Pulse width was set to 100 μs. Cathodic and anodic phases were separated by a 100 μs interphase delay, used in stimulation protocols to lower excitation thresholds and enhance nerve fiber recruitment (van den Honert and Mortimer; 1979; Gorman and Mortimer; 1983). The anodic discharge was designed to last for 15 ms to ensure full discharge of the capacitor, followed by a stand-by phase before the next pulse to avoid phase switch artifacts. Total duration of a single pulse was 20 ms, resulting in a 50 Hz pulse frequency.

Table 1: *k-values and corresponding cathodic currents, charge densities using geometric surface area, real charge densities considering electrode roughness, and real k-values*

k -	**Cathodic current** (mA)	**Charge density** ($\mu C/cm^2$)	**Real charge density** ($\mu C/cm^2$)	**Real *k*** -
0.566	8.5	4.33	3.36	0.46
1.25	18.5	9.41	7.3	1.13
1.55	26.4	13.44	10.42	1.44
1.66	30	15.26	11.84	1.55
1.75	33.2	16.92	13.11	1.64
1.85	37.3	18.99	14.73	1.74
2	44.3	22.57	17.49	1.89

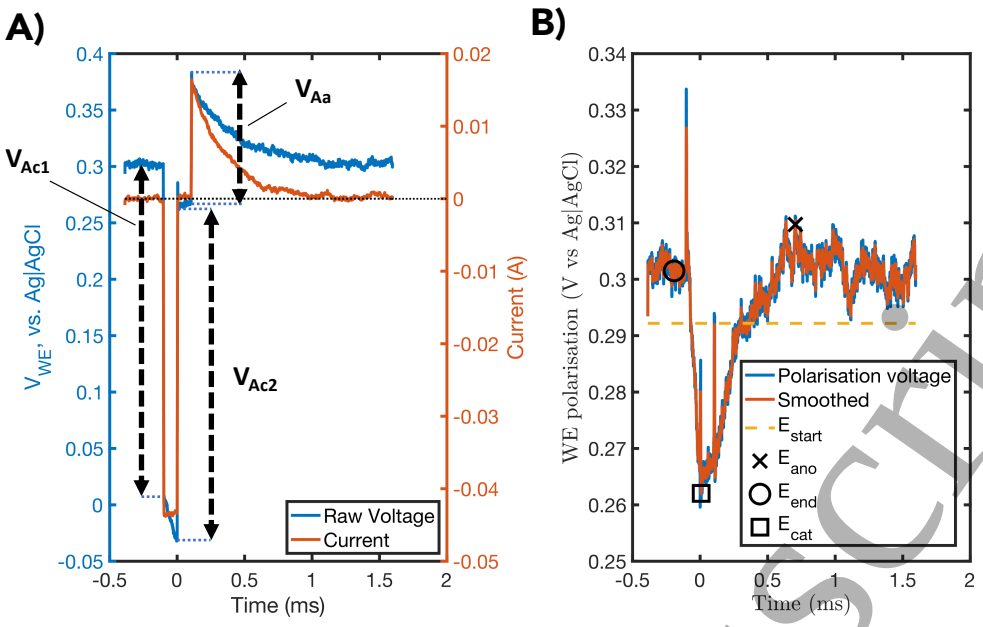

Figure 2: *Examples of A) raw working electrode potential (blue) and current (red) waveforms, with access voltages indicated by arrows, and B) polarisation curve, where the access voltages were removed from the raw potential measurement, and how E_{ano}, E_{end} and E_{cat} are read. In A) a black dotted line indicates the zero-current line.*

The cathodic current was measured by voltage drop across a 100 Ω current measurement resistor using an oscilloscope (10 MΩ probes, 5 orders of magnitude larger than the source impedance). The working electrode (WE) potential was measured versus the Ag|AgCl reference electrode (RE) with a differential probe (Pico®, 47 $M\Omega$ input impedance, also 5 orders of magnitude larger than the source impedance). The data were analysed with custom Matlab (MathWorks, R2022a) scripts. Four potentials were of particular interest and were recorded for each k-value to monitor potential evolution with increasing charge injection: potential before the start of the pulse train (E_{start}), potential at the beginning of the last pulse (E_{end}), maximum anodic polarisation observed during the last pulse (E_{ano}) and minimum cathodic polarisation observed during the last pulse (E_{cat}), see Fig. 2. E_{ano} and E_{cat} are polarisation potentials, meaning that the ohmic polarisation (or access voltage) in the electrolyte was removed from the observed electrode potentials before reading the polarisation potentials: changes in electrode current are accompanied by

instantaneous changes in electrode voltage due to Ohm's law and the uncompensated electrolyte resistance R_u which do not represent the true electrochemical potential of the electrode interface (Cogan; 2008). As we can see on Fig. 2 A), the anodic access voltage V_{Aa} is different from the cathodic access voltages V_{Ac1} and V_{Ac2}, as previously reported (Cogan; 2008), therefore we estimated the three access voltages separately to have the most accurate polarisation curve. Some inaccuracies remained in the polarisation curve in the form of spikes, which were ignored when reading the polarisation potentials. E_{end} was recorded at the beginning of the last pulse rather than after the last pulse to avoid reporting a potential during the 15 ms anodic discharge phase, which may have not stabilised. Furthermore, it is expected that potential ratcheting is minimial between the 999^{th} and 1000^{th} pulses, as an equilibrium between cathodic and anodic irreversibly injected charge mechanisms would have been established after a few pulses (Merrill et al.; 2005; Kumsa et al.; 2016).

For the pulsing experiment, electrodes were disconnected from a Gamry 600+ potentiostat, which was performing the conditioning sequence (see 2.3), and connected to a custom stimulator through toggle switches. The evolution of the open-circuit potential (OCP) was monitored during the switching phase until stabilized.

2.3. Electrochemical characterisation

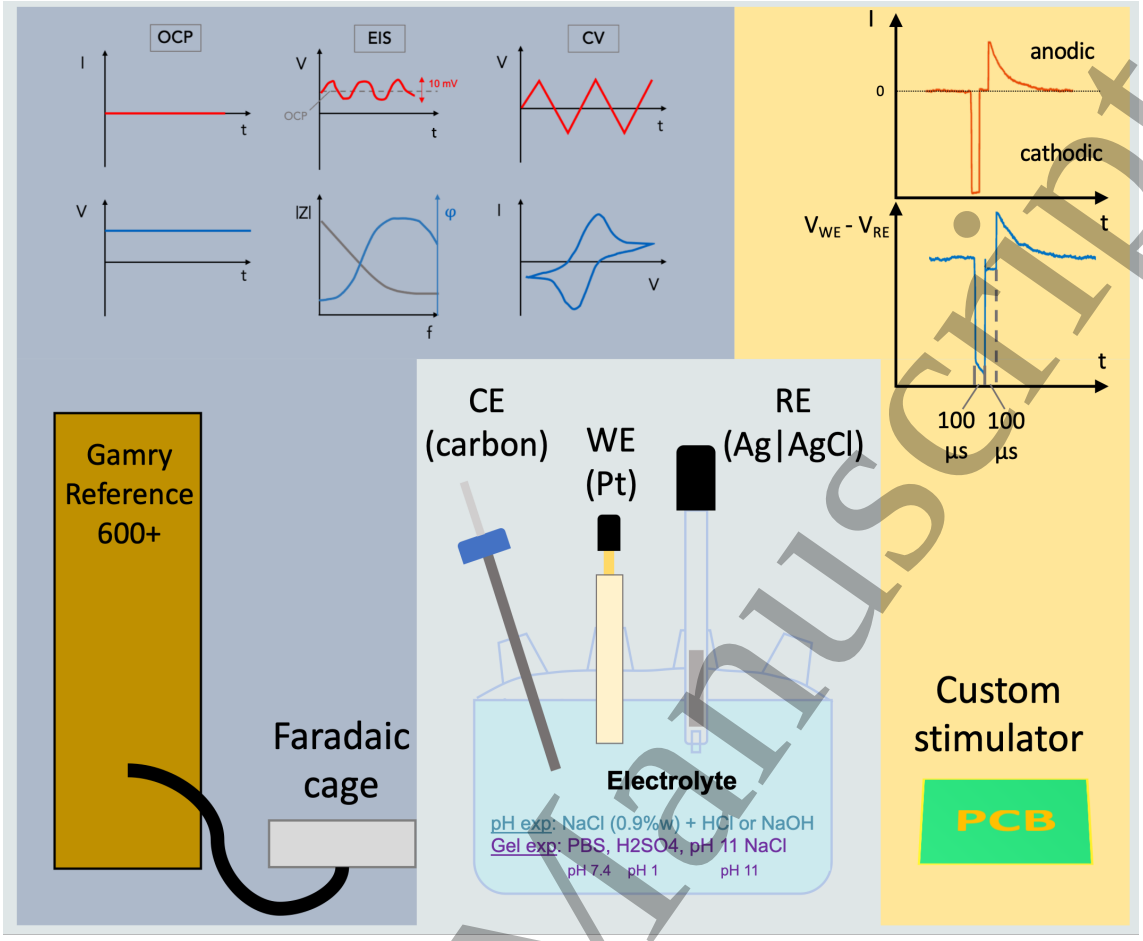

Figure 3: *Experimental setup schematic. The dark blue area represents the electrochemical testing part, the yellow area represents the stimulation part. After electrochemical tests, a train of 1000 pulses was applied with a custom stimulator (see waveforms in the top right corner) and the working electrode potential was recorded on an oscilloscope (not shown on the schematic).*

A three-electrode setup was used, a 5 mm-diameter platinum disk WE (geometric surface area = 19.635 mm^2, Roughness factor 1.29), an Ag|AgCl RE and a carbon rod counter electrode (CE), were placed in a 150 mL chamber (Pine Research RRPG310), see Fig. 3. The WE roughness was determined using the charge of hydrogen adsorption in sulfuric acid and dividing by the theoretical value of $Q_H = 210\,\mu C/cm^2$ (Topalov et al.; 2014; Weltin et al.; 2019), which yielded a roughness factor of 1.29, hence a real surface area of 25.3 mm^2. Before being placed in solution, the WE surface was cleaned with acetone and isopropyl alcohol.

Electrochemical characterization was conducted with a Gamry 600+ potentiostat. Cleaning and electrode conditioning of platinum electrodes were shown to be crucial for accurate and repeatable potential readings (Hudak et al.; 2017; Lai et al.; 2019; Weltin and Kieninger; 2021; Doering et al.; 2023). Therefore, to characterize the electrode-electrolyte interface and to keep the interface in a repeatable "base state", a series of electrochemical tests including cyclic voltammetry was run systematically between pulse trains.

Open-circuit potential

Open-circuit potential (OCP) measurements were intercalated between characterisation tests to allow the WE potential to stabilise. OCP measurement durations were determined empirically checking the rate of change, with the same durations used consistently for subsequent experiments.

Electrochemical impedance spectroscopy

Electrochemical impedance spectroscopy (EIS) was performed at OCP with a 5 mV_{p-p} amplitude across a frequency sweep from 1 Hz to 100 kHz.

Cyclic voltammetry

Cyclic voltammetry (CV) was performed with a sweep rate of 100 $mV.s^{-1}$ until the voltammogram was stable, typically for 20 cycles, across the water window. The water window was determined empirically for each electrolyte by running a test CV before the experiment, identifying the regions of water electrolysis and delimiting the potential range when the current exceeded $\pm$ 200 μA ($\approx$ 0.01 $mA.cm^2$). CVs started from OCP by a oxidation sweep and finished at 0 V vs Ag|AgCl, leaving an oxide-free surface and minimising polarisation (Harris et al.; 2022). We hypothesise that the stabilisation period placed between the CV and the pulsing trains allowed the interface to recover a natural oxide coverage.

Experimental procedure

All electrochemical characterisation tests and the pulsing test were assembled in a 9-step sequence to ensure maximal repeatability. An initial characterisation

sequence (steps (i) to (vii)) was performed to establish the base state at the interface, and the same sequence was used between pulsing tests to characterise possible changes and reestablish the base state. Steps (i) to (viii) were performed with the potentiostat and step (ix) with the custom stimulator:

(i) OCP for 30 minutes to allow the WE potential to stabilize and the surface to hydrate;
(ii) EIS pre CV;
(iii) OCP for 2 minutes;
(iv) CV for 20 cycles;
(v) OCP for 15 minutes to allow the WE potential to stabilize again;
(vi) EIS post CV;
(vii) OCP for 2 minutes;
(viii) OCP for 10 minutes during which the electrodes are connected to the stimulator;
(ix) Pulsing experiment, 1000 biphasic pulses at 50 Hz, $\approx$ 20 s;
(x) Adjust current level and repeat from step (i).

3. Results

3.1. Electrode-electrolyte interface stability

For reliable comparisons between results the electrode-electrolyte interface needed to return to a consistent state between pulsing experiments. The conditioning sequence was developed with that intention, with CV reestablishing the surface state through repetitive oxidation and reduction, and EIS and OCP used to monitor for interface changes. We do not assume that stable EIS and OCP implies that no surface dissolution occurs, instead that the surface is returned to a similar starting condition between current-controlled pulse trains to allow for comparison between sequential experimental steps.

The first conditioning CV, performed before the first pulse train, decreased the high-frequency impedance of electrodes (not shown). After a change following the first conditioning CV, the EIS response remained consistent, neither CV nor pulse

trains affected the EIS values, showing that the interface conditioning protocol was suitable.

Fig. 4 shows the relationship between measured OCP and pH and compares the trend to the Nernstian response. Each data point corresponds to the average of stabilised OCP values after pulsing trains (n = 7, OCP taken at the end of the first step of the testing sequence). Mean and variability of OCP within experiments (OCP after each pulsing test, n = 7) are given in the supplementary material figure **??**. OCP remained stable throughout experiments, with a maximum standard deviation of ±11.75 mV within a single pulsing test series (typically conducted in a single day of experimentation). For each pulsing test series, the mean OCP was plotted against pH (Fig. 4) to verify that OCP varied with pH following Nernst's relation. A linear fit yielded a gradient of -48.1 $mV.pH^{-1}$ such that the expected Nernstian response, –59 $mV.pH^{-1}$, was not within the 95% confidence interval (CI) [-53 $mV.pH^{-1}$; -43 $mV.pH^{-1}$] due to large residuals observed at low pH. A fit excluding pH < 4 showed a gradient of -56.2 $mV.pH^{-1}$ with a 95% CI of [-62 $mV.pH^{-1}$; -50 $mV.pH^{-1}$], hence a Nernstian response.

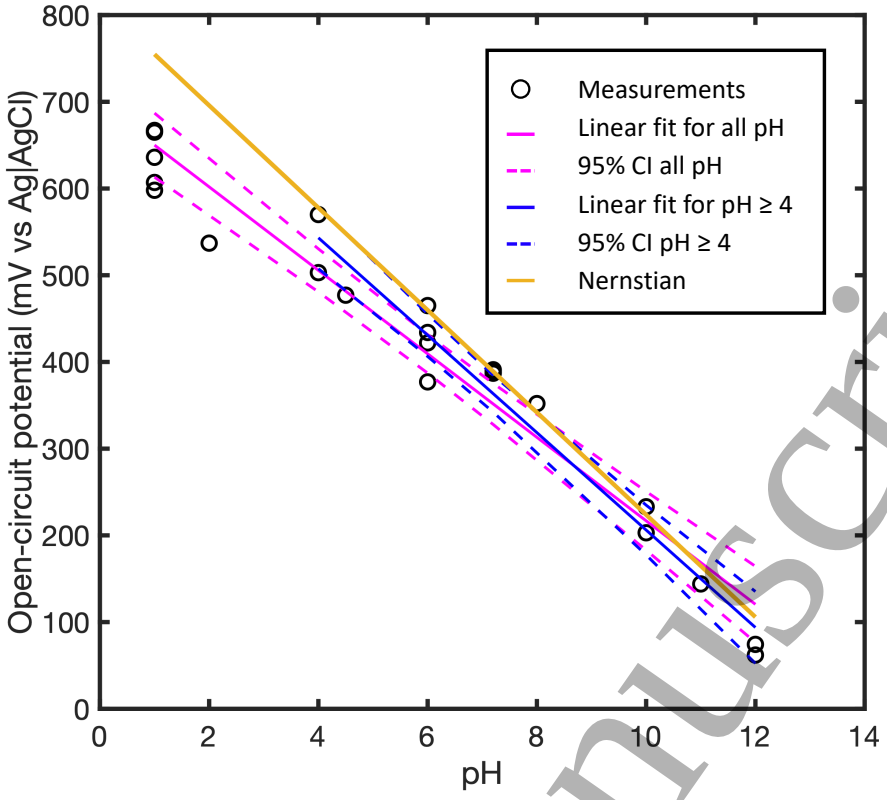

Figure 4: *Experimental open-circuit potential values plotted against pH and compared with Nernst's equation. Linear fits are represented with their respective 95% confidence intervals.*

Gelation of the electrolyte with agar generally yielded a lower mean OCP except for PBS by 22.5 mV on average (average of mean(E_{sol}) - mean(E_{gel})), see Table 2.

Table 2: *Mean average OCP and standard deviation (std) within experiments for each electrolyte in solution and gel form.*

Electrolyte	PBS		H_2SO_4	
pH	7.4		1	
Gel or **S**olution	S	G	S	G
OCP (mV)	284.1±7.69	281.9±29.43	607.3±9.21	584.9±8.61
Electrolyte	NaCl			
pH	11		1	
Gel or **S**olution	S	G	S	G
OCP (mV)	196.5 ± 1.87	175.3±2.36	568.6±10.31	524.2±1.10

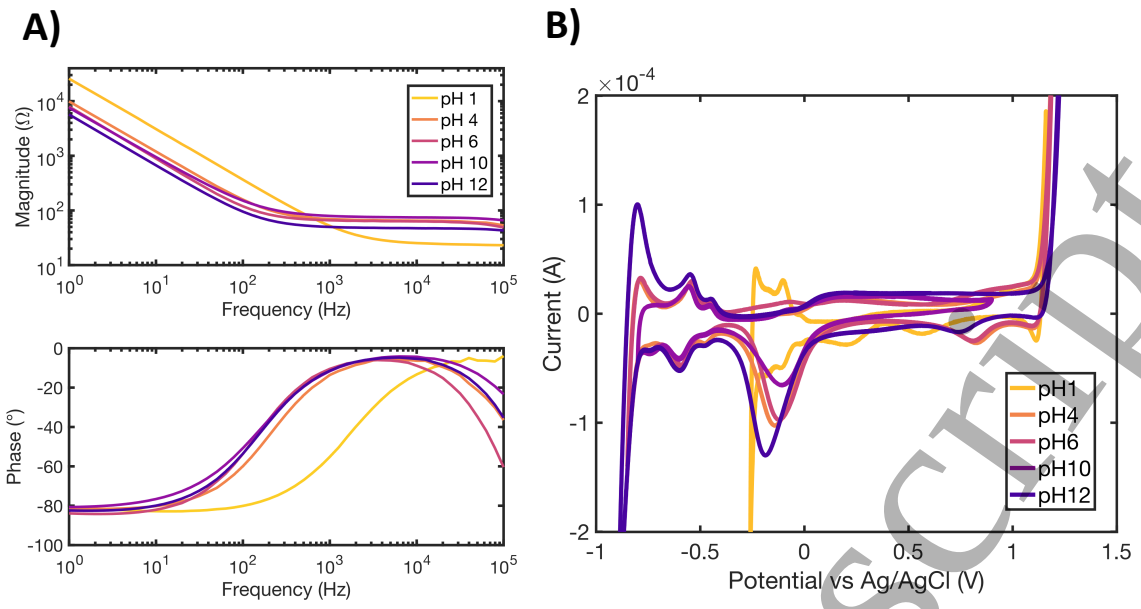

Figure 5: *A. Bode plot of the impedance spectrum for isotonic saline solutions of pH from 1 to 12 with impedance magnitude at the top and phase at the bottom. B. Cyclic voltammograms for solution electrolytes of pH from 1 to 12.*

Saline solutions from pH 4 to pH 12 showed similar impedance Bode plots (Fig. 5A.), with only a slightly lower impedance at high frequencies (f > 1 kHz) for pH 12. pH 1 was substantially different, showing a 2 to 3 times lower impedance at high frequencies and transitioning to capacitive behaviour at higher frequencies than other pH values, by about one order of magnitude. Gelation of the electrolyte with agar did not change the EIS graphs at a concentration of 0.5% w/v (not shown). Higher concentrations increased the high-frequency impedance (not shown), attributed to air trapped at the electrode surface.

CVs were stable throughout pulsing experiments. CVs were expected to exhibit similar peaks, only shifted along the potential axis according to Nernst's relation (Fig. 5B.). pH 1 H-evolution and pH 12 O-evolution were expected to differ from other pH values. pH 1 and 12 had narrower water windows than pH 4, 6 and 10, which exhibited similar voltammograms. pH 1 was shifted towards higher potential as expected, and the pH 1 voltammogram showed differences in the H-evolution region (E < 0 V vs Ag|AgCl), exhibiting a wider voltammogram in that region and

peaks closer to one another, and an oxide reduction peak split into two distinct peaks (E ≈ 0.2 V and E ≈ 0.55 V). For pH 12, and slightly less for pH 10, 6 and 4, H-peaks were more spaced due to a scarcer presence of H^+ ions, with higher overpotentials for H^+ ion interactions with the electrode surface (Ledezma-Yanez et al.; 2017).

3.2. Evolution of peak potential with k for various pH

The WE potential at the last (1000^{th}) pulse was higher than at the first pulse, which indicates positive potential ratcheting (Fig. 6). Potential ratcheting is characteristic of asymmetrical charge injection mechanisms between the cathodic and anodic phase, leading to more irreversible charge injection in one phase, causing changes in the electrode-electrolyte interface potential. When starting from OCP, with a cathodic-first pulse, in an oxygen containing medium, the electrode potential moves negatively into the oxygen reduction reaction region, which is generally believed to be irreversible because the reaction products move away from the electrode surface and are not available for oxidation: hence the ratcheting positive (Merrill et al.; 2005).

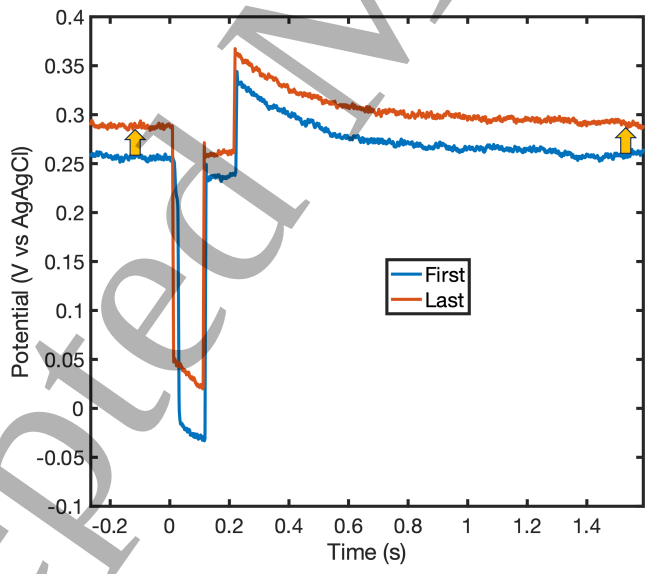

Figure 6: *Working electrode potential in PBS (pH = 7.4) during the first and last (1000^{th}) pulses of the pulse train, uncorrected for ohmic drop. The gradual increase in potential, or potential ratcheting, is shown by arrows.*

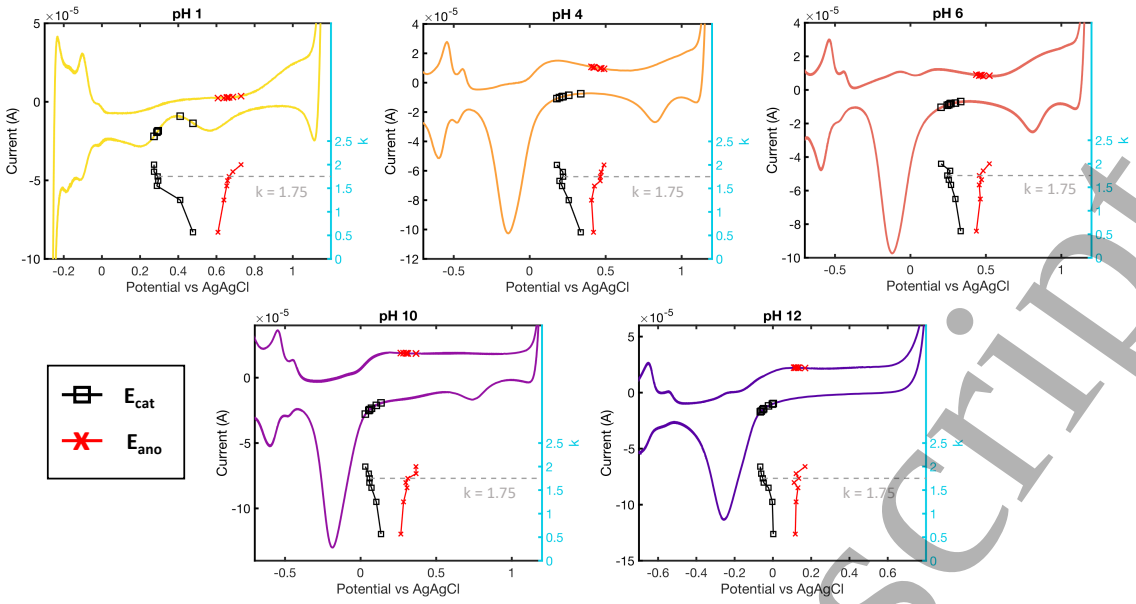

Figure 7: *Evolution of peak anodic potential (red) and peak cathodic potential (black) with k in saline solutions of pH from 1 to 12 and location on the respective cyclic voltammogram (100 mV.s^{-1}). Shannon's limit k = 1.75 is indicated by a dashed grey line.*

The maximum anodic potential (E_{ano}) was positively correlated with k. E_{ano} increased gradually with k, at a steeper rate for higher k-values (Fig. 7). The trends are similar for all pH values, especially for pH 1, 6, and 12. In comparison, pH 4 transitions to a steeper increase at a lower k-value ($k \approx 1.3$ vs. $k \approx 1.7$ for other pH values), and pH 10 shows a step increase around $k \approx 1.75$ between two linear evolution regions. For every pH, E_{ano} was located in the oxide formation region independently of k, which suggests that even though E_{ano} increased with k and showed some steeper variations around Shannon's damage limit, the same electrochemical mechanism was available for charge injection.

The minimum cathodic potential (E_{cat}) was negatively correlated with k (Fig. 7). A decrease of E_{cat} with k was expected as increasing k equates to increasing i (Eq 2), thus driving the potential more negative. At all pH except pH 1, the trend was similar with a steady decrease of E_{cat} with k, pH 6 and 12 showing a slightly steeper decrease from $k \approx 1.5$. At pH 1, E_{cat} decreased steeply at $k \leq 1.5$, then decreased at a much slower rate, almost plateauing. The location of E_{cat}

on the voltammogram is interesting: while E_{cat} for pH 4 and 6 was between two peaks independent of k, pH 1, 10 and 12 E_{cat} entered an oxide reduction peak around Shannon's damage limit $k = 1.75$. The mechanism is apparent for pH 1 where E_{cat} transitions from one peak to the other, showing that there is a change of electrochemical mechanism when a certain amount of charge is injected.

3.3. Evolution of peak potential with k for gelated electrolytes

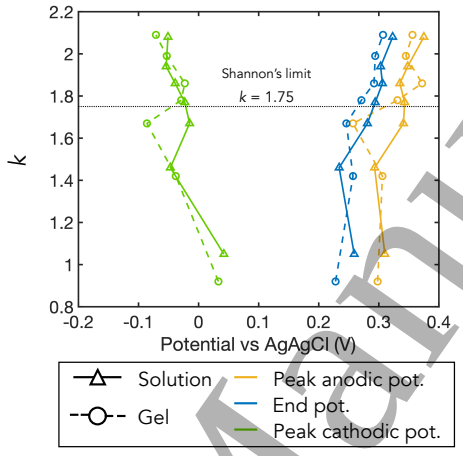

Figure 8: *Evolution of peak anodic potential (yellow), peak cathodic potential (green), and end potential (blue) with k in gelated vs solution PBS (pH = 7.4). Shannon's limit k = 1.75 is indicated by a dotted line.*

E_{ano} and E_{cat} showed similar evolutions with k for gel and solution in four different electrolytes, for example in PBS in Fig. 8. E_{ano} and E_{cat} were not significantly different with 95% confidence by two-sample Kolmogorov-Smirnov test (data not shown). Plotting potential excursions (E_{ano} or E_{cat}) in gel electrolytes against solution electrolytes showed a substantial discrepancy in E_{cat} (Fig. 9). While the linear fit was almost superimposed with the identity line ($E_{gel} = E_{sol}$) for E_{ano} ($E_{gel} = 0.959\,E_{sol}$, 95% C.I. [0.856; 1.061]), the E_{cat} linear fit showed a steeper gradient ($E_{gel} = 1.294\,E_{sol}$, 95% C.I. [1.094; 1.493]), which left the identity line outside the 95% CI. The four electrolytes figure as separate groups, with pH 11 saline at the bottom (gel E_{cat} < sol E_{cat}) and H_2SO_4 and pH 1 saline at the top (gel E_{cat} > sol

391 E_{cat}), which indicates a cumulative effect of electrolyte gelation and pH.

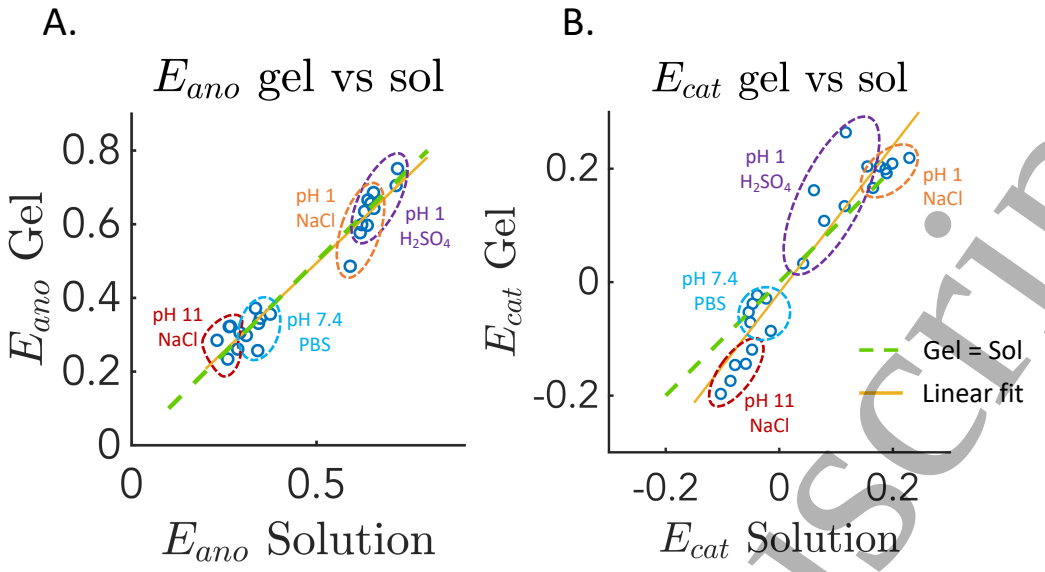

Figure 9: *Direct comparison of A) anodic and B) cathodic polarisation potentials in gel electrolytes vs solutions. Each data point is a pair (E_{gel};E_{sol}) for the same k-value. A linear fit of all data points is shown (yellow line) and compared $E_{gel} = E_{sol}$ (green dotted line).*

392 E_{ano} and E_{cat} were placed on cylic voltammograms for gel electrolytes, similarly
393 to what was done with pH solutions (Fig. 10). CVs of gel electrolytes showed similar
394 peaks to solution electrolytes but less defined, suggesting an alteration of reaction
395 kinetics. For all electrolytes, E_{ano} was consistently located in the oxide formation
396 region and E_{cat} was consistently located in the oxide reduction region. Despite
397 a noticeable oxidation peak starting at E $\approx$ 0.6 V, E_{ano} of H_2SO_4 gel and pH 1
398 saline gel and solution varied almost linearly with k, as did the E_{cat}, and H_2SO_4
399 solution showed a linear increase in E_{cat} and a step increase in E_{ano} around $k = 1.75$,
400 entering an oxidation peak. H_2SO_4 solution behaviour is similar to the observations
401 of Kumsa et al. (2016) and different than pH 1 saline for example, showing that
402 electrodes in H_2SO_4 may have a different charge injection behaviour than in saline
403 electrolytes.

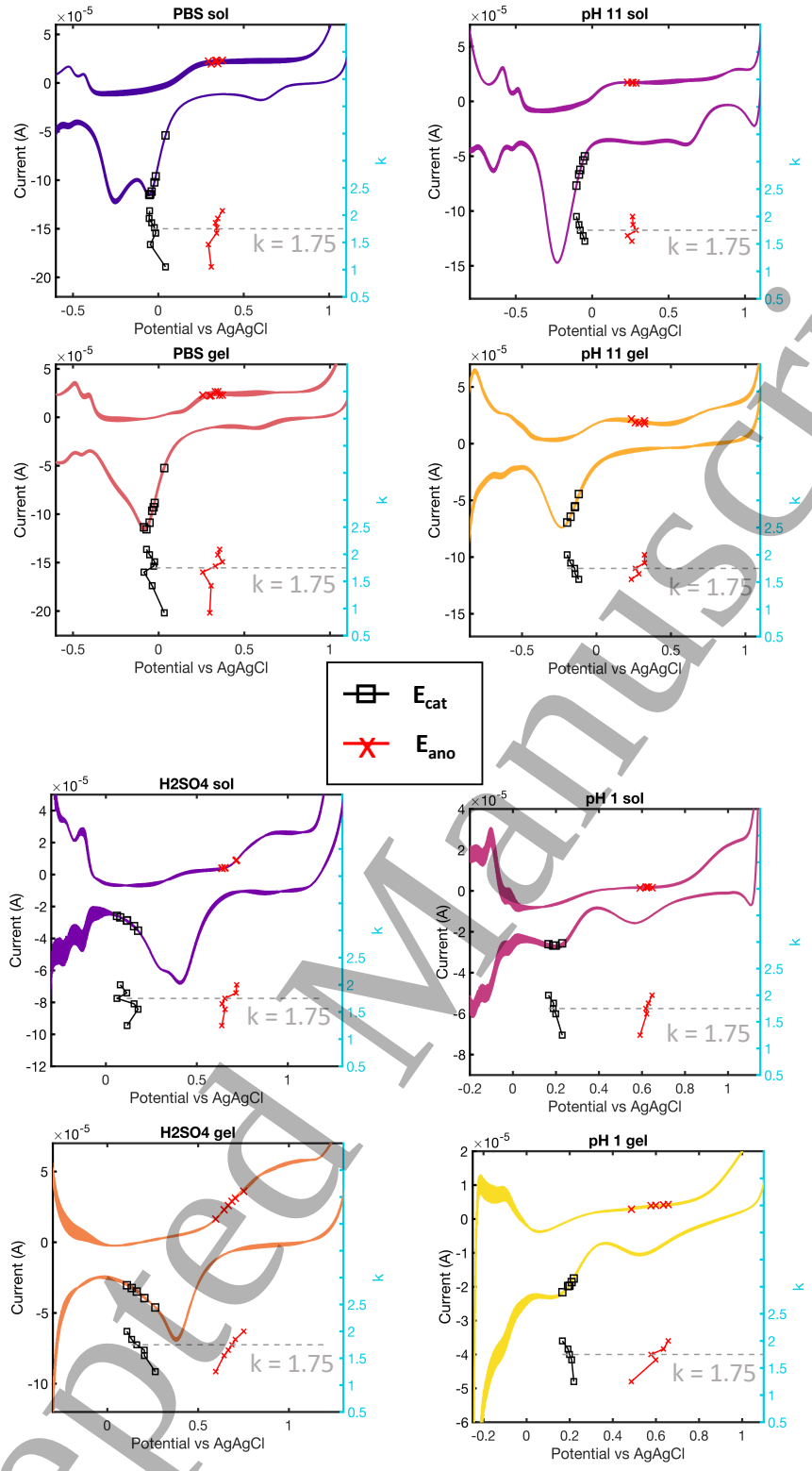

Figure 10: *Evolution of peak anodic potential (red) and peak cathodic potential (black) with k in gelated vs solution electrolytes and location on the respective cyclic voltammogram (100 $mV.s^{-1}$). Shannon's limit $k = 1.75$ is indicated by a dashed grey line.*

4. Discussion

This paper studied the influence of two characteristics of the tissue surrounding implanted electrodes as an electrolyte, pH and gel structure, on charge injection and especially damage mechanisms. It was found that when the injected charge approached the safe limit determined by Shannon (1992), the electrode potential entered a region favourable for platinum oxide reduction during the cathodic phase, while being in the platinum oxide formation region during the anodic phase. Electrolyte gelation showed a substantial effect on cathodic potentials, while close to none on anodic potentials, which may affect damage mechanisms.

4.1. Electrochemical impedance spectroscopy

The high-frequency impedance decrease observed after the first CV cycles is hypothesised to be due to electrochemical surface cleaning and surface activation following repeated oxidations and reductions. CV caused a conditioning of the surface, achieving a reproducible state, which explains why the EIS did not change through further stimulation. The lower high-frequency impedance and high-frequency transition to capacitive behaviour observed for pH 1 are attributed to the greater H^+ ion concentration, which have a high affinity with the electrode surface since H^+ ions participate in pseudocapacitive charge injection through H-plating (Puglia and Bowen; 2022). The evolution of calculated double-layer capacitance values with pH was counter-intuitive, as one would expect a higher capacitance in acidic pH, due to the increased presence of H^+ ions, which act as a pseudo-capacitance on platinum.

4.2. Cyclic voltammetry

The voltammograms present some differences to typical CVs reported in literature. Often, the baseline current in the H-evolution region is noticeably negative due to oxygen reduction (Musa et al.; 2011; Hudak et al.; 2010). Here, the baseline current was effectively more negative in that region, but the shift was not very sharp, due to the large electrode size (Weltin and Kieninger; 2021). The water window for isotonic

saline [-0.9 V;+1.2 V] was wider than the usually reported [-0.6 V;+0.9 V] window in PBS, however, wider windows have been reported in the literature (Boehler et al.; 2020) and may be due to crystallographic structures and electrode surface states (Weltin and Kieninger; 2021). The water window is also known to be wider in NaCl (Hudak et al.; 2017). The absence of pH shift for pH 4, 6 and 10 is counter-intuitive but has been observed in fundamental electrochemistry: Strbac (2011) swept the potential on a Pt rotating disk electrode and found that diffusion limited currents were different for pH < 3.5 and pH > 10 but no difference was observed in between. In low buffer concentrations, outside of extreme solution pH, the local pH at the electrode surface converges to a stable value, without changing the global solution pH. Therefore, even if the solution pH is measured at various values, the local pH will converge to the stable value, different from the solution pH and the electrode behaviour will remain unchanged (Strbac; 2011; Li et al.; 2013; Briega-Martos et al.; 2020).

The cleaning protocol was designed to leave the electrode surface with a natural partial oxide coverage, which may influence the charge injection mechanisms during pulsing, as electrode conditioning and experimental protocols may influence the ratio of oxidation and reduction charge injection capacity (Musa et al.; 2011; Harris et al.; 2018a) and electrode behaviour, demonstrating more influence than the presence of dissolved oxygen for instance (Doering et al.; 2023). The technique used in this work to let the OCP return to a stable value after stopping the CV at 0 V yielded OCPs sufficiently stable for comparison; however, OCP variability may have been reduced by carefully controlling the electrode potential with a potentiostatic step following CV, as implemented by Doering et al. (2023). The protocol was slightly modified for experiments comparing gel and solution electrolytes, with a 20 minute step (i) instead of 30 minutes (the potential could still stabilise in that time), 10 instead of 20 CV cycles (voltammograms were stable after 6-7 cycles), and suppression of steps (ii) and (iii) as EIS did not change after the first CV. Thus, it is possible that the results observed for pH 1 and pH 11 saline in the gel vs solution experiment were slightly different than the pH experiment because of the modified protocol; such

discrepancy is expected to be minor, since CVs and OCP traces were similar before and after the protocol modification.

4.3. Evolution of peak potentials

Shannon's damage threshold has been associated with platinum oxide formation in studies performed in sulfuric acid (Kumsa et al.; 2016) and subcutaneously in rats (Kumsa et al.; 2017), which showed that above a charge injection threshold, platinum oxide is likely formed, which would eventually result in platinum dissolution (Kumsa et al.; 2016), which may cause subsequent neural damage (Agnew et al.; 1977). In this work, we reproduced the same approach in alternative electrolytes to understand how electrolyte characteristics affect charge injection mechanisms near Shannon's limit, thereby extending the validity of our understanding of electrode behaviour near Shannon's limit. Unbuffered saline solutions were used for a variety of reasons. First, the electrode behaviour discrepancy between *in vitro* and *in vivo* may be explained by the imperfect buffering capacity in the body, which has been shown to be overestimated by PBS (Harris et al.; 2019) and may be temporarily exhausted locally during neural stimulation (Weltin and Kieninger; 2021). Second, since the body buffer may be exhausted at the electrode surface, pH changes may arise, which may change the electrode behaviour, and using unbuffered saline allowed us to voluntarily steer the pH across a wide range to study its influence. pH shift is not considered as a major source of neural damage, as pH is regulated by the body's buffers and the pH showed to steer away from 7.4 only in the first few μm away from the electrode (Ballestrasse et al.; 1985; Huang et al.; 2001). However, the pH shift at the electrode surface may be significant (> 3) (Ballestrasse et al.; 1985), and pH is known to affect electrochemical reactions at the electrode surface including Pt dissolution (Topalov et al.; 2014), therefore, local pH shifts may generate different reaction paths, and possibly different reaction mechanisms by altering reaction kinetics. Huang et al. (2001) compared the pH shifts at Pt electrodes during biphasic stimulation in PBS, unbuffered saline and *in vivo*, and demonstrated that pH shifted by 1 pH unit at 0.2 mm from the electrode surface both

in saline and *in vivo*. These results were achieved at a stimulation equivalent to $k \approx 1.36$, at 1000 pulses per second, with the pH shift shown to depend on stimulation intensity, pulse frequency, and distance of the pH sensor to the electrode. Our experiments have larger stimulation intensity (up to 10 times) and 20 times fewer pulses, so we expect increased magnitude of pH shifts close to the electrode, as suggested by Huang et al. (2001) and Ballestrasse et al. (1985). Huang et al. (2001) also showed that buffering the electrolyte cancelled the pH shift, as did a series capacitor. Thus in this study, we apply a stimulus that we expect would cause a pH shift at the electrode surface; however, our addition of a series capacitor for anodic discharge, may have cancelled the effective pH shifts we wanted to study. Therefore, to study the effect of a pH shift on the charge injection mechanisms in this pulsing regime, we used unbuffered saline, manually adjusted the pH across a wide range, and measured the potential excursions in these conditions.

In this work, we also use the same analysis strategy as Kumsa et al. (2016) by using CVs to localise electrode polarisations during pulsing and identify possible electrochemical reactions. There are three main anodic reactions for Pt electrodes in chloride (Cl^-) containing electrolytes: hydrogen (H) desorption, platinum oxide (PtO) formation, and adsorbed Cl^- oxidation through chloride complexation, which is outside of traditional water window ($E^0 \approx 0.95\,V$ vs Ag|AgCl (Geiger et al.; 2015)) for Pt but may be reached in acidic media. The anodic polarisation were recorded in the PtO formation peak for all pH and all k-values, which shows that PtO formation is the main faradaic reaction supplying anodic current. The cathodic reaction path is more complex to determine, as there are several competing processes that may occur, including mainly PtO reduction, reduction of molecular oxygen (O_2) and Cl^- adsorption. It is likely that both reactions occur during pulsing, and Cogan et al. (2010) and Musa et al. (2011) evaluate contribution of molecular O_2 reduction respectively at 7% in O_2-saturated saline on 25 μmm diameter electrodes and 19-34% in ambient O_2 concentration on 50 μm diameter electrodes. Dissolved O_2 was present in the electrolytes we used at ambient conditions (21%), therefore it may contribute to charge injection during pulsing. We observed positive potential ratcheting,

indicating a cathodically-biased imbalanced irreversible charge injection, meaning more irreversible charge was injected during the cathodic phase. The imbalance is observed in the polarisation curve (Fig 2 B)) in the form of a potential overshoot in the anodic phase, which would not be present with a completely reversible charge injection, and is most likely due to molecular oxygen reaction.

Molecular oxygen reduction and PtO reduction contributions are superimposed on a CV (-0.6 V $< E_{O_2} <$ +0.05 V, vs $E_{PtO} \approx 0.1$ V), where the cathodic polarisation was found. We hypothesise molecular oxygen reduction to be a source of cathodic irreversible charge injection ; however, the change of behaviour observed around Shannon's damage limit is related to the onset potential of PtO reduction, whereas O_2 reduction is present for all k-values. Indeed, for pH 1, 10, and 12, the cathodic polarisation enters the PtO reduction peak for the highest values of k, suggesting a correlation between Shannon's damage limit and the onset of PtO reduction. Topalov et al. (2014) studied Pt dissolution mechanisms by varying anodic and cathodic potential extremes separately during cyclic voltammetry. Topalov et al. (2014) showed that increasing the upper limit of the CV did not affect anodic dissolution greatly but had a significant effect on cathodic dissolution, which was explained by a larger PtO coverage created, so a larger amount of PtO for reduction: amount of Pt dissolution was proportional to oxide coverage. Therefore, we hypothesise the following compound mechanism: molecular O_2 reduction causes irreversible cathodic charge injection, which drives the potential more positive through potential ratcheting. As a consequence, the anodic potential is driven further into the PtO formation region, leading to larger oxide coverage, and at k-values approaching Shannon's limit of $k = 1.75$, PtO reduction occurs at a substantial rate, which yields toxic levels of platinum dissolution. These findings support our hypothesis about the importance of the cathodic potential in dissolution mechanisms.

This interpretation supplements the findings by Kumsa et al. (2016), which suggested that the tipping point for Shannon's damage limit was the onset of PtO formation during the anodic phase. In this work, we did not observe substantial

changes in the available anodic reactions when k exceeded the damage limit, as E_{ano} was consistently found inside the oxide formation peak, independent of k. The PtO formation region is a broad peak (0.1 V$\leq$ E $\leq$ 0.9 V), which is able to supply substantial anodic charge, and may explain the relatively small variation in E_{ano}. The combination of E_{cat} entering oxide reduction and E_{ano} reaching oxide formation creates cycles of oxidation-reduction of platinum to platinum oxide, which eventually leads to platinum dissolution (Doering et al.; 2022). Therefore, we suggest that the tipping point explaining neural damage as observed by McCreery et al. (1990) is when the electrode potential enters the PtO reduction region during the cathodic phase.

In pH 1, the cathodic behaviour was substantially different that other pH, with the cathodic polarisation clearly transitioning from one reduction peak to another, more negative, peak. Cl^- is known to adsorb onto platinum and compete particularly with Pt oxidation, and this phenomenon is enhanced by electrolyte acidity (Hudak et al.; 2017; Doering et al.; 2022). It is possible that in pH 1 saline, we observed another Pt dissolution path, as Cl^- interfering the cyclic oxidation-reduction process of Pt (possibly blocking some dissolved Pt redeposition) is enhanced at low pH (Geiger et al.; 2015). *In vivo*, this phenomenon is less likely to take place, as proteins such as albumin adsorb onto Cl^- preferential adsorption sites (Hudak et al.; 2017).

If we accept the hypothesis that Shannon's limit is correlated with harmful faradaic reactions, then one of the main flaws of Shannon's relationship needs to be addressed to make Shannon's relationship suitable for new electrode designs: the absence of roughness consideration. Indeed, Shannon's relationship (eq 1) uses the electrode's geometric surface area, however, techniques have been developed since which allow to increase the electrochemically available area, including laser roughening (Green et al.; 2012) or Pt black deposition (Arcot Desai et al.; 2010). With such surface treatments, the charge injection mechanisms would be altered for a given geometric current density, especially with increased double-layer capacitance, which would enable more non-faradaic charge injection. Therefore, an adapted version of Shannon's limit may be appropriate, based on electrochemical surface

area, rather than geometric. In the present work, we report a roughness factor of 1.29, which yielded inferior real k-values by roughly 0.1 compared to geometric k-values (Table 1). As roughness was not reported in the studies on which Shannon's relationship is based, it is not possible to suggest the real charge densities and real k-values. k is correlated with $-log\ R_f$ (R_f being the roughness factor): from Eq 1, $D = \frac{Q}{S} = \frac{Q}{R_f S_{geo}}$, with S_{geo} the geometrical surface area. Thus, doubling the roughness factor would only make k smaller by 0.3. Therefore, we suggest caution in the use of Shannon's limit, in particular for roughened electrodes, and the use of a region between of real k around 1.75 rather than a hard limit, as Shannon (1992) recommended, and as our results seem to show, with a shift in mechanisms between $k \approx 1.5$ and $k \approx 1.85$.

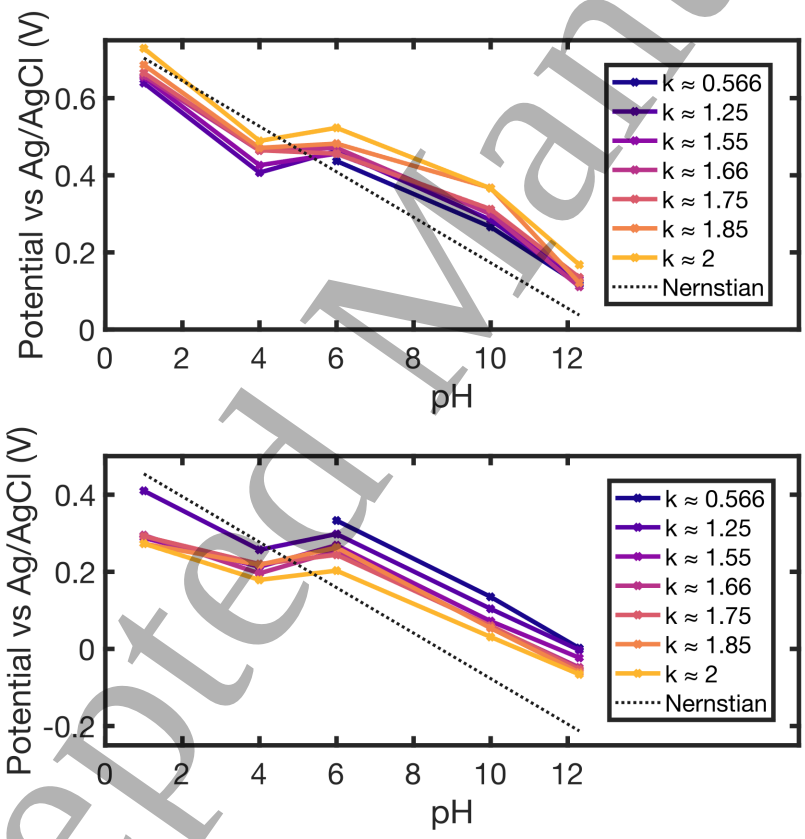

Figure 11: *Evolution of peak anodic potential (top) and peak cathodic potential (bottom) with pH (solution electrolytes) for all values of k and comparison with Nernst's equation.*

The evolution of E_{ano} and E_{cat} with respect to pH was analysed separately for each k-value in Fig. 11. E_{ano} followed Nernst's equation closely with a mean average gradient of -42.1 ± 1.59 $mV.pH^{-1}$ (see Table **??**), and Nernst's gradient inside the 95% C.I. for 6 out of 7 k-values (except $k = 0.566$). E_{cat} presented a less steep mean gradient of -31.7 ± 4.52 $mV.pH^{-1}$, with Nernst's gradient outside the 95% C.I. for all k-values. pH 4 and 6 showed similar E_{ano} and E_{cat}, which marked a plateau in the E vs pH plots.

There is a similarity between the pH experiment and the gel versus solution experiment: E_{ano} followed the expected trend, respectively Nernst's relation for the pH study and gel = solution for the gelation study, but E_{cat} exhibited a different slope, indicating that E_{cat} is more influenced by electrolyte properties. Except for proton adsorption/desorption, Pt anodic and cathodic reaction paths are asymmetrical, therefore different behaviours of cathodic and anodic polarisation can be expected. The gel structure may limit mass transport, which may affect molecular O_2 reduction, which is the only mass-transport limited cathodic reaction (Merrill et al.; 2005). Gels also induce larger polarisations, which may affect faradaic reactions in presence, without substantially changing CVs. While PBS and pH 1 saline had similar cathodic behaviour between gels and solutions, pH 11 saline gels showed consistently more negative E_{cat} than solutions and pH 1 sulfuric acid consistently higher E_{cat} in gels. Thus, in basic electrolytes, a larger polarisation was needed to deliver the same charge, and a lower polarisation in acidic electrolytes. Basic electrolytes have lower concentrations of H^+, which is consumed in both cathodic reactions (molecular oxygen reduction and PtO reduction, which may explain the overpotential discrepancy. However, the amount of O_2 reduction did not vary significantly as Eano, which characterises the degree of irreversibility remained highly similar. We also noticed that a smaller overpotential was only noticed for H_2SO_4, not for similar pH NaCl with HCl, which suggests that gel electrolytes may indeed affect Pt dissolution processes. Pt dissolution was shown to be affected by pH, being more prominent in acidic media (Topalov et al.; 2014; Doering et al.;

2022) and occurring at higher rates in sulfuric acid than perchloric acid (Topalov et al.; 2014). Our results may indicate that gels exacerbate the influence of pH and influence Pt dissolution mechanisms, decreasing the necessary polarisation in favorable acidic conditions (for sulfuric acid) increasing the necessary polarisation in defavorable basic conditions. Gels may act as a positive feedback loop, further favoring Pt dissolution processes in acidic media, as the decreased overpotentials suggest, and hindering the same processes in basic media, where larger overpotentials were required. The exact mechanism by which the feedback loop is created is unknown, however, it could be due to hindered diffusion in gels, creating different local environments at the electrode surface, depending on pH. In this paper, we make the case that E_{cat} in association with E_{ano}, rather than E_{ano} alone drives damage mechanisms at platinum electrodes, hypothesising that the difference in slope of E_{cat} with pH compared to E_{ano} relates to the relationship of E_{cat} with damage mechanisms, whereas E_{ano} follows Nernst's relation. Therefore, the discrepancy between gels and solutions in E_{cat} may indicate that gelation affects the cathodic charge injection mechanisms and may therefore affect damage mechanisms. The effect of reduced buffering capacity and restricted diffusion should be studied more in detail to further understand the behaviour of platinum electrodes *in vivo*, especially concerning damage mechanisms.

5. Conclusion

In this work, we studied the influence of electrolyte pH and electrolyte gelation on charge injection mechanisms related to Shannon's safe stimulation limit, using a custom experimental setup. The setup showed accurate, stable and repeatable potential measurements and electrochemical characterisation. Potential ratcheting was observed, indicating an imbalance in irreversible charge injection mechanisms between the cathodic and anodic phases, with higher cathodic irreversible charge injection due to molecular oxygen reduction. The maximum anodic electrode potential was systematically located in the oxide formation region, while the minimum cathodic electrode potential entered the oxide reduction only when k

approached Shannon's damage limit, independently of solution pH. We hypothesise that the irreversibility caused by molecular oxygen reduction causes increased anodic potential and thus platinum oxide formation, which increases the magnitude of platinum oxide reduction in the cathodic phase; when approaching Shannon's limit, a substantial amount of platinum is undergoing repeated cycles of oxidation and reduction, dissolving the electrode material and possibly releasing noxious products in the electrode surroundings. Therefore the results showed here support previous hypotheses identifying platinum dissolution as the damage mechanism behind Shannon's limit.

Although gelation of the electrolyte did not appear to affect potential excursions during stimulation, a comparison showed that cathodic potentials were behaving substantially differently in gels compared with solutions at the same pH values, although it was not statistically significant. Since the minimum cathodic potential is key for Shannon's limit, gelation of the electrolyte may have an effect on damage mechanisms, which needs to be investigated further. Understanding how extracellular matrix-mimicking gel electrolytes affect charge injection mechanisms would benefit the development and testing of neural electrodes and help bridge the gap between bench-tests and in vivo stimulation.

Conflict of Interest

TN, AV, and HL have no conflicts of interest to declare.

Ethics statement

This study does not report work involving humans, animals, or human or animal tissues.

Acknowledgements

The authors thank the Institute of Physics and Engineering in Medicine (IPEM, UK) for funding equipment used in this study.

References

Agnew, W. F., McCreery, D. B., Yuen, T. G. and Bullara, L. A. (1989). Histologic and physiologic evaluation of electrically stimulated peripheral nerve: considerations for the selection of parameters, *Annals of biomedical engineering* **17**(1): 39–60.

Agnew, W. F., Yuen, T. G. and McCreery, D. B. (1983). Morphologic changes after prolonged electrical stimulation of the cat's cortex at defined charge densities, *Experimental neurology* **79**(2): 397–411.

Agnew, W. F., Yuen, T. G., Pudenz, R. H. and Bullara, L. A. (1977). Neuropathological effects of intracerebral platinum salt injections, *Journal of Neuropathology & Experimental Neurology* **36**(3): 533–546.

Agnew, W., Yuen, T., McCreery, D. and Bullara, L. (1986). Histopathologic evaluation of prolonged intracortical electrical stimulation, *Experimental Neurology* **92**(1): 162–185.

Arcot Desai, S., Rolston, J. D., Guo, L. and Potter, S. M. (2010). Improving impedance of implantable microwire multi-electrode arrays by ultrasonic electroplating of durable platinum black, *Frontiers in neuroengineering* **3**: 1303.

Ballestrasse, C. L., Ruggeri, R. T. and Beck, T. R. (1985). Calculations of the pH changes produced in body tissue by a spherical stimulation electrode, *Annals of biomedical engineering* **13**(5): 405–424.

Boehler, C., Carli, S., Fadiga, L., Stieglitz, T. and Asplund, M. (2020). Tutorial: guidelines for standardized performance tests for electrodes intended for neural interfaces and bioelectronics, *Nature protocols* **15**(11): 3557–3578.

Briega-Martos, V., Ferre-Vilaplana, A., Herrero, E. and Feliu, J. M. (2020). Why the activity of the hydrogen oxidation reaction on platinum decreases as ph increases, *Electrochimica Acta* **354**: 136620.

Butterwick, A., Vankov, A., Huie, P., Freyvert, Y. and Palanker, D. (2007). Tissue damage by pulsed electrical stimulation, *IEEE Transactions on Biomedical Engineering* **54**(12): 2261–2267.

Campbell, A. and Wu, C. (2018). Chronically implanted intracranial electrodes: tissue reaction and electrical changes, *Micromachines* **9**(9): 430.

Cogan, S. F. (2008). Neural stimulation and recording electrodes, *Annu. Rev. Biomed. Eng.* **10**: 275–309.

Cogan, S. F., Ehrlich, J., Plante, T. D., Gingerich, M. D. and Shire, D. B. (2010). Contribution of oxygen reduction to charge injection on platinum and sputtered iridium oxide neural stimulation electrodes, *IEEE transactions on biomedical engineering* **57**(9): 2313–2321.

Cogan, S. F., Ludwig, K. A., Welle, C. G. and Takmakov, P. (2016). Tissue damage thresholds during therapeutic electrical stimulation, *Journal of neural engineering* **13**(2): 021001.

Craggs, M., Donaldson, N. d. N. and Donaldson, P. (1986). Performance of platinum stimulating electrodes, mapped on the limitvoltage plane: Part 1 charge injection in vivo, *Medical and Biological Engineering and computing* **24**: 424–430.

DiLorenzo, D. J., Jankovic, J., Simpson, R. K., Takei, H. and Powell, S. Z. (2014). Neurohistopathological findings at the electrode–tissue interface in long-term deep brain stimulation: systematic literature review, case report, and assessment of stimulation threshold safety, *Neuromodulation: Technology at the Neural Interface* **17**(5): 405–418.

Doering, M., Kieninger, J., Kübler, J., Hofmann, U., Rupitsch, S. J., Urban, G. and Weltin, A. (2023). Advanced electrochemical potential monitoring for improved understanding of electrical neurostimulation protocols, *Journal of Neural Engineering* .

Doering, M., Kieninger, J., Urban, G. A. and Weltin, A. (2022). Electrochemical microelectrode degradation monitoring: in situ investigation of platinum corrosion at neutral ph, *Journal of Neural Engineering* **19**(1): 016005.

Donaldson, N. d. N. and Donaldson, P. (1986a). Performance of platinum stimulating electrodes mapped on the limitvoltage plane: Part 2 corrosion in vitro, *Medical and Biological Engineering and Computing* **24**: 431–438.

Donaldson, N. d. N. and Donaldson, P. (1986b). When are actively balanced biphasic

('lilly') stimulating pulses necessary in a neurological prosthesis? i historical background; pt resting potential; q studies, *Medical and Biological Engineering and Computing* **24**: 41–49.

Geiger, S., Cherevko, S. and Mayrhofer, K. J. (2015). Dissolution of platinum in presence of chloride traces, *Electrochimica Acta* **179**: 24–31.

Gorman, P. H. and Mortimer, J. T. (1983). The effect of stimulus parameters on the recruitment characteristics of direct nerve stimulation, *IEEE Transactions on Biomedical Engineering* (7): 407–414.

Green, R. A., Hassarati, R. T., Bouchinet, L., Lee, C. S., Cheong, G. L., Jin, F. Y., Dodds, C. W., Suaning, G. J., Poole-Warren, L. A. and Lovell, N. H. (2012). Substrate dependent stability of conducting polymer coatings on medical electrodes, *Biomaterials* **33**(25): 5875–5886.

Gupta, A. K., Zygun, D. A., Johnston, A. J., Steiner, L. A., Al-Rawi, P. G., Chatfield, D., Shepherd, E., Kirkpatrick, P. J., Hutchinson, P. J. and Menon, D. K. (2004). Extracellular brain pH and outcome following severe traumatic brain injury, *Journal of neurotrauma* **21**(6): 678–684.

Harris, A. R., Newbold, C., Carter, P., Cowan, R. and Wallace, G. G. (2018a). Charge injection from chronoamperometry of platinum electrodes for bionic devices, *Journal of The Electrochemical Society* **165**(12): G3033–G3041.

Harris, A. R., Newbold, C., Carter, P., Cowan, R. and Wallace, G. G. (2018b). Measuring the effective area and charge density of platinum electrodes for bionic devices, *Journal of neural engineering* **15**(4): 046015.

Harris, A. R., Newbold, C., Carter, P., Cowan, R. and Wallace, G. G. (2019). Using chronopotentiometry to better characterize the charge injection mechanisms of platinum electrodes used in bionic devices, *Frontiers in Neuroscience* **13**.

Harris, A. R., Newbold, C., Stathopoulos, D., Carter, P., Cowan, R. and Wallace, G. G. (2022). Comparison of the in vitro and in vivo electrochemical performance of bionic electrodes, *Micromachines* **13**(1): 103.

Huang, C. Q., Carter, P. M. and Shepherd, R. K. (2001). Stimulus induced ph

changes in cochlear implants: an in vitro and in vivo study, *Annals of biomedical engineering* **29**: 791–802.

Hudak, E. M. (2011). *Electrochemical evaluation of platinum and diamond electrodes for neural stimulation*, PhD thesis, Case Western Reserve University.

Hudak, E. M., Kumsa, D. W., Martin, H. B. and Mortimer, J. T. (2017). Electron transfer processes occurring on platinum neural stimulating electrodes: calculated charge-storage capacities are inaccessible during applied stimulation, *Journal of neural engineering* **14**(4): 046012.

Hudak, E., Mortimer, J. and Martin, H. (2010). Platinum for neural stimulation: voltammetry considerations, *Journal of Neural Engineering* **7**(2): 026005.

Johnson, M. D., Kao, O. E. and Kipke, D. R. (2007). Spatiotemporal ph dynamics following insertion of neural microelectrode arrays, *Journal of neuroscience methods* **160**(2): 276–287.

Kumsa, D. W., Bhadra, N., Hudak, E. M. and Mortimer, J. T. (2017). Electron transfer processes occurring on platinum neural stimulating electrodes: pulsing experiments for cathodic-first, charge-balanced, biphasic pulses for $0.566 \leq k \leq 2.3$ in rat subcutaneous tissues, *Journal of Neural Engineering* **14**(5): 056003.

Kumsa, D. W., Hudak, E. M., Bhadra, N. and Mortimer, J. T. (2019). Electron transfer processes occurring on platinum neural stimulating electrodes: pulsing experiments for cathodic-first, charge-imbalanced, biphasic pulses for $0.566 \leq k \leq 2.3$ in rat subcutaneous tissues, *Journal of Neural Engineering* **16**(2): 026018.

Kumsa, D. W., Montague, F. W., Hudak, E. M. and Mortimer, J. T. (2016). Electron transfer processes occurring on platinum neural stimulating electrodes: pulsing experiments for cathodic-first/charge-balanced/biphasic pulses for $0.566 \leq k \leq 2.3$ in oxygenated and deoxygenated sulfuric acid, *Journal of neural engineering* **13**(5): 056001.

Kuncel, A. M. and Grill, W. M. (2004). Selection of stimulus parameters for deep brain stimulation, *Clinical neurophysiology* **115**(11): 2431–2441.

Lai, B.-C., Wu, J.-G. and Luo, S.-C. (2019). Revisiting background signals and the

electrochemical windows of au, pt, and gc electrodes in biological buffers, *ACS Applied Energy Materials* **2**(9): 6808–6816.

Ledezma-Yanez, I., Wallace, W. D. Z., Sebastián-Pascual, P., Climent, V., Feliu, J. M. and Koper, M. (2017). Interfacial water reorganization as a ph-dependent descriptor of the hydrogen evolution rate on platinum electrodes, *Nature Energy* **2**(4): 1–7.

Leung, R. T., Shivdasani, M. N., Nayagam, D. A. and Shepherd, R. K. (2014). In vivoandin vitrocomparison of the charge injection capacity of platinum macroelectrodes, *IEEE Transactions on Biomedical Engineering* **62**(3): 849–857.

Li, M. F., Liao, L. W., Yuan, D. F., Mei, D. and Chen, Y.-X. (2013). ph effect on oxygen reduction reaction at pt (1 1 1) electrode, *Electrochimica Acta* **110**: 780–789.

Lilly, J. C., Hughes, J. R., Alvord Jr, E. C. and Galkin, T. W. (1955). Brief, noninjurious electric waveform for stimulation of the brain, *Science* **121**(3144): 468–469.

McCreery, D., Agnew, W., Yuen, T. and Bullara, L. (1988). Comparison of neural damage induced by electrical stimulation with faradaic and capacitor electrodes, *Annals of biomedical engineering* **16**(5): 463–481.

McCreery, D., Agnew, W., Yuen, T. and Bullara, L. (1995). Relationship between stimulus amplitude, stimulus frequency and neural damage during electrical stimulation of sciatic nerve of cat, *Medical and Biological Engineering and Computing* **33**: 426–429.

McCreery, D. B., Agnew, W. F., Yuen, T. G. and Bullara, L. (1990). Charge density and charge per phase as cofactors in neural injury induced by electrical stimulation, *IEEE Transactions on Biomedical Engineering* **37**(10): 996–1001.

McCreery, D., Pikov, V. and Troyk, P. R. (2010). Neuronal loss due to prolonged controlled-current stimulation with chronically implanted microelectrodes in the cat cerebral cortex, *Journal of neural engineering* **7**(3): 036005.

McHardy, J., Robblee, L., Marston, J. and Brummer, S. (1980). Electrical

stimulation with Pt electrodes. IV. factors influencing Pt dissolution in inorganic saline, *Biomaterials* **1**(3): 129–134.

Merrill, D. R., Bikson, M. and Jefferys, J. G. (2005). Electrical stimulation of excitable tissue: design of efficacious and safe protocols, *Journal of neuroscience methods* **141**(2): 171–198.

Mortimer, J. T. and Bhadra, N. (2018). Fundamentals of electrical stimulation, *Neuromodulation*, Elsevier, pp. 71–82.

Musa, S., Rand, D. R., Bartic, C., Eberle, W., Nuttin, B. and Borghs, G. (2011). Coulometric detection of irreversible electrochemical reactions occurring at pt microelectrodes used for neural stimulation, *Analytical chemistry* **83**(11): 4012–4022.

Puglia, M. K. and Bowen, P. K. (2022). Cyclic voltammetry study of noble metals and their alloys for use in implantable electrodes, *ACS omega* **7**(38): 34200–34212.

Renz, A. F., Reichmuth, A. M., Stauffer, F., Thompson-Steckel, G. and Vörös, J. (2018). A guide towards long-term functional electrodes interfacing neuronal tissue, *Journal of neural engineering* **15**(6): 061001.

Robblee, L., McHardy, J., Agnew, W. and Bullara, L. (1983). Electrical stimulation with Pt electrodes. VII. dissolution of pt electrodes during electrical stimulation of the cat cerebral cortex, *Journal of neuroscience methods* **9**(4): 301–308.

Shannon, R. V. (1992). A model of safe levels for electrical stimulation, *IEEE Transactions on biomedical engineering* **39**(4): 424–426.

Strbac, S. (2011). The effect of pH on oxygen and hydrogen peroxide reduction on polycrystalline Pt electrode, *Electrochimica Acta* **56**(3): 1597–1604.

Topalov, A. A., Cherevko, S., Zeradjanin, A. R., Meier, J. C., Katsounaros, I. and Mayrhofer, K. J. (2014). Towards a comprehensive understanding of platinum dissolution in acidic media, *Chemical Science* **5**(2): 631–638.

Tykocinski, M., Shepherd, R. K. and Clark, G. M. (1995). Reduction in excitability of the auditory nerve following electrical stimulation at high stimulus rates, *Hearing research* **88**(1-2): 124–142.

van den Honert, C. and Mortimer, J. T. (1979). The response of the myelinated nerve fiber to short duration biphasic stimulating currents, *Annals of biomedical engineering* **7**: 117–125.

Vatsyayan, R., Cleary, D., Martin, J. R., Halgren, E. and Dayeh, S. A. (2021). Electrochemical safety limits for clinical stimulation investigated using depth and strip electrodes in the pig brain, *Journal of neural engineering* **18**(4): 046077.

Weltin, A., Ganatra, D., König, K., Joseph, K., Hofmann, U. G., Urban, G. A. and Kieninger, J. (2019). New life for old wires: electrochemical sensor method for neural implants, *Journal of Neural Engineering* **17**(1): 016007.

Weltin, A. and Kieninger, J. (2021). Electrochemical methods for neural interface electrodes, *Journal of Neural Engineering* **18**(5): 052001.

Yuen, T. G., Agnew, W. F., Bullara, L. A., Jacques, S. and McCreery, D. B. (1981). Histological evaluation of neural damage from electrical stimulation: considerations for the selection of parameters for clinical application, *Neurosurgery* **9**(3): 292–299.